# Iridescence of Patterned Carbon Nanotube Forests on Flexible Substrates: From Darkest Materials to Colorful Films

**Kun-Che Hsieh,[†] Tsung-Yen Tsai,[‡] Dehui Wan,[†] Hsuen-Li Chen,[†,*] and Nyan-Hwa Tai[‡,*]**

[†]Department of Materials Science and Engineering, National Taiwan University, Taipei, Taiwan, and [‡]Department of Materials Science and Engineering, National Tsing Hua University, Hsinchu, Taiwan

**ABSTRACT** In this study, we prepared carbon nanotube (CNT) forests exhibiting two types of optical properties: so-called "darkest materials" and films displaying iridescence phenomena. The darkest materials, comprising vertically aligned CNT (VA-CNT) forests, displayed extremely low reflections as a result of the rough surface and the trapping of light in the CNT forests. The lengths of the CNTs in the CNT forests had a strong influence on whether the light transmitted through the CNT forest or reflected from the substrate. From an investigation of the limitations of the darkest materials of CNT forests, we prepared CNT surfaces running the gamut from dark materials to iridescent. To study iridescence phenomena, we prepared two kinds of patterns of CNT forests on flexible polycarbonate substrates: CNTs arrayed in hexagonal-hole patterns and broccoli-like CNTs, the latter formed through a combination of inverse nanosphere lithography (INSL) and a poisoned-catalyst mechanism. In the patterned CNT forests, even though the refractive index difference between the CNT film and air was extremely low and even though the CNTs could trap the incident light, the iridescence phenomenon remained, inducing colorful images from the CNT films.

**KEYWORDS:** carbon nanotubes (CNTs) · darkest material · iridescence · flexible substrates · inverse nanosphere lithography

Carbon nanotubes (CNTs) attract a great deal of attention because of their unique properties as nanomaterials. In recent years, several theoretical studies have been published regarding the optical properties of aligned CNT films. In 1997, Vidal *et al*. presented an effective medium approach to analyze the optical properties of CNT films.[1] They also developed the Maxwell−Garnett (MG) approach to study composite films of aligned CNTs. The MG approach appears to be a good approximation for systems in which the CNTs are separated by large and intermediate distances. The consideration of full electromagnetic (EM) wave coupling between the CNTs was essential when studying the close-packed structures that appear in aligned CNT films.[2] The good agreement between the numerical and experimental data revealed that this MG model was a useful tool for analyzing the optical properties of CNTs. Acros *et al*. also used reflectivity measurements in the visible range to investigate the optical properties of vertically aligned CNTs.[2] With graphite as the host medium and air as the inclusion substance, they developed an effective medium layer (EML) method to determine the thickness and effective refractive index of aligned-CNT films. Although the effective refractive indexes of CNT films can be determined through the fitting of reflectance spectra, their effective extinction coefficients have not been reported previously—even though refractive indices and extinction coefficients are two important factors influencing the optical behavior of CNT films.

Recently, few theoretical calculations[1,3] and experimental measurements[2,3] revealed that materials displaying extremely low refractive indices ($n = 1.01-1.10$) could be prepared using low-density CNT arrays. Such nanotube arrays can be viewed as extremely black objects because of their low reflection and high absorption.[3] Besides, a rough surface of other materials also reveals an ultralow reflection due to the random scattering.[4−7] Yang *et al*. reported that low-density aligned nanotubes exhibit high absorption coefficients in the direction parallel to the CNTs and, more importantly, extremely low refractive indices for light in the visible wavelength regime.[8] This arrangement provides a material having a rough surface with no repeating topology, causing light to scatter in random directions and, thereby, making the surface extremely black. Arrays of vertically aligned carbon nanotubes (VA-CNTs) can also exhibit such properties through a mechanism for minimizing reflection that is fundamentally different from that of conventional antireflection coatings or roughened surfaces. Nevertheless, arrays of VA-CNTs films might have limitations when used to prepare extremely dark materials. To understand these

*Address correspondence to hsuenlichen@ntu.edu.tw, nhtai@mx.nthu.edu.tw.

Received for review August 5, 2009 and accepted February 09, 2010.

**Published online February 25, 2010.** 10.1021/nn901910h

limitations, in this study we investigated the optical properties of CNT films, including their refractive indices, extinction coefficients, and interference and diffraction phenomena.

The special optical characteristics of periodical nanostructures have attracted much interest in both the physical and biological sciences.[9−12] Nanopatterned CNT arrays have potential applications in many fields, for example, as field emission displays, biosensors, energy storage systems, and photonic devices. Controlling the density of nanopatterned CNTs can enhance the field emission properties of devices, for example, by preventing CNT cathodes from undergoing screen effects.[13−15] In this study, we also transferred the nanopatterned CNTs onto flexible substrates to increase their practicality in the applications requiring flexible devices.

Typically, the nanopatterning method used for the fabrication of CNT arrays involves electron-beam (E-beam) lithography, an expensive and time-consuming process. Recently, nanosphere lithography (NSL) was developed as an effective and economical fabrication technique; self-assembled monolayers of polystyrene (PS) spheres are used as a mask to form patterned catalysts, which can then be adopted for the growth of aligned and spatially controlled CNT arrays and ZnO nanorods.[16−18] Using NSL, several two-dimensional periodical nanostructures have been demonstrated, including nanobowl,[19,20] nanotube,[21−23] nanorod,[18,24] nanohoneycomb,[25] and nanoscale ring arrays.[26] In the NSL method, a monolayer of PS spheres covers a substrate as a mask layer; the presence of boundaries in the monolayer of PS spheres is inevitable.[27] After depositing the catalyst, the PS monolayer is removed from the substrate. The catalyst layer is, therefore, arranged on the defect positions of the honeycomb patterns; CNTs can grow from these defect positions.

To the best of our knowledge, the special iridescence phenomena of patterned VA-CNT films have not been reported previously. Iridescence is an optical phenomenon in which the hue changes with respect to the angle from which the surface is viewed; it is seen in such systems as soap bubbles and butterfly wings. Iridescence is caused by multiple reflections from multilayered, semitransparent surfaces in which phase shifts and the interference of reflections modulate the incident light by amplifying or attenuating some frequencies more than others. In this study, we used a patterned template and inverse NSL lithography to fabricate patterned CNT forests on flexible substrates. To investigate the limitations of CNT forests as extremely dark materials, we examined the optical properties of VA-CNT films to further understand their optical phenomena. In addition to preparing extremely dark materials, we also observed iridescence from patterned CNT forests, which can be applied in flexible devices, such as solar cells and displays featuring shiny decorations.

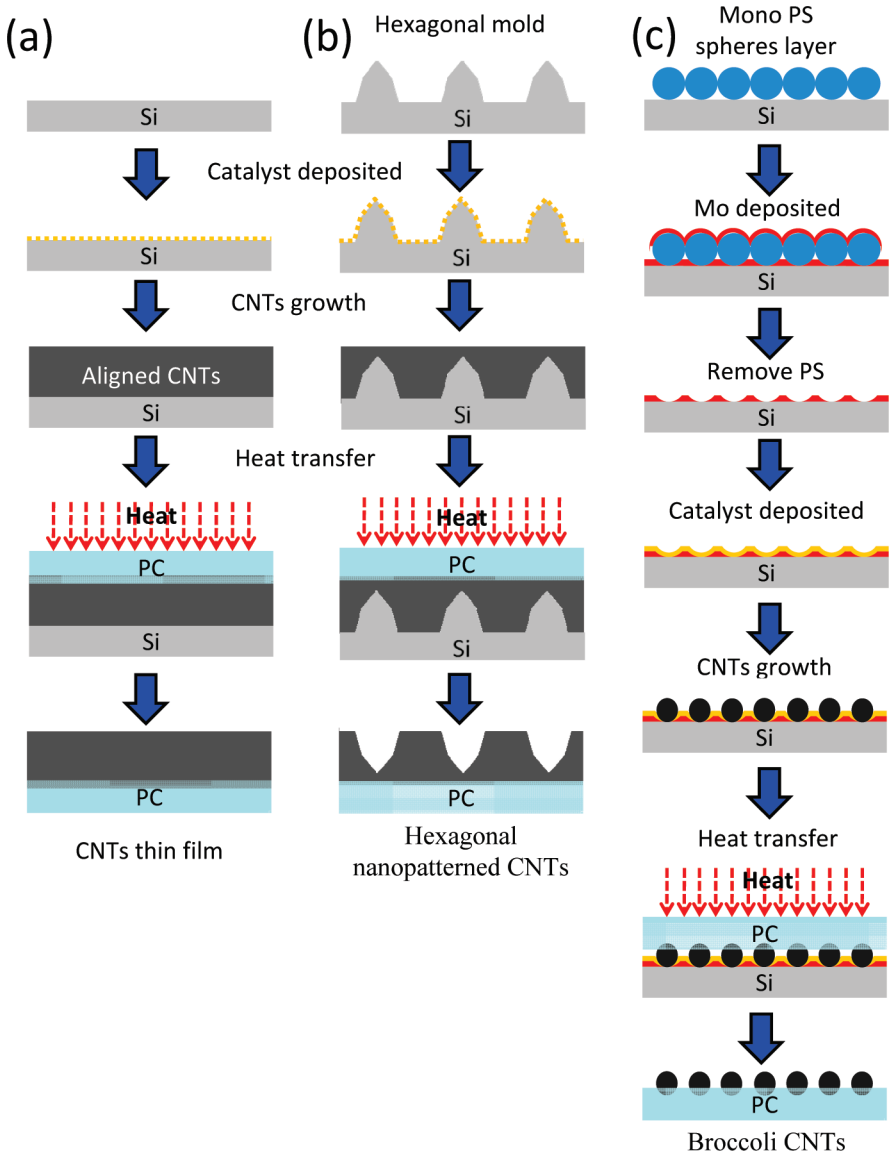


**Figure 1. Schematic representations of the processing of (a) VA-CNTs, (b) CNTs aligned with hexagonal holes, and (c) broccoli-shaped CNTs on flexible substrates.**

## RESULTS AND DISCUSSION

Figure 1 displays schematic representation of the processes used

to pattern VA-CNTs on flexible substrates. The fabrication procedures are described in the Methods section in detail. Figure 1a illustrates the preparation of the flat VA-CNT films[28,33] and the transfer of the CNT films from the Si substrates to flexible polycarbonate (PC) substrates. The CNT forest grown on the patterned template is displayed schematically in Figure 1b. To fabricate the broccoli-shaped CNTs, a monolayer of PS spheres was defined as the template, as displayed in Figure 1c. The lengths of VA-CNTs were affected significantly by the growth temperature. Figure 2 panels a, b, c, and d display VA-CNTs having heights of 0.5, 2, 8, and 80 μm that we synthesized at temperatures of 500, 600, 700, and 800 °C, respectively. The densities of these VA-CNTs were in the range from $10^{11}$ to $10^{12}$ $cm^{-2}$, as depicted in the enlarged SEM images. According to the SEM images of the CNT films, the densities of these four VA-CNT films were all similar. Moreover, the growth temperature controlled the growth rates of the CNT films, allowing us to obtain CNTs of various lengths. Besides, these CNT films with various lengths show similar roughness values of *ca.* 15−20 nm. The transparencies of the VA-CNT films of different thicknesses are revealed in the bottom photographs in Figures 2a−d. The letters "CNT" printed under the VA-CNTs on the PC substrates gradually became opaque upon increasing the length of the CNTs. That is, the absorption of the VA-CNTs films increased upon increasing the length of the CNTs, thereby inhibiting the light from passing through the CNT forest.

We further investigated the optical properties of the VA-CNTs to understand the reasons for the extreme darkness of the VA-CNTs, using the EML model to consider the VA-CNT films as graphite-based materials featuring air as the inclusion material. The optical behavior of such a layer can be calculated using the effective medium approximation. In particular, we selected the Bruggemann approximation,[29] which can be used in those cases where the content of inclusion material is large with respect to that of the host, as was the case in our systems. The effective optical behavior of a layer is described by the following combination of optical constants of the host and inclusion materials:

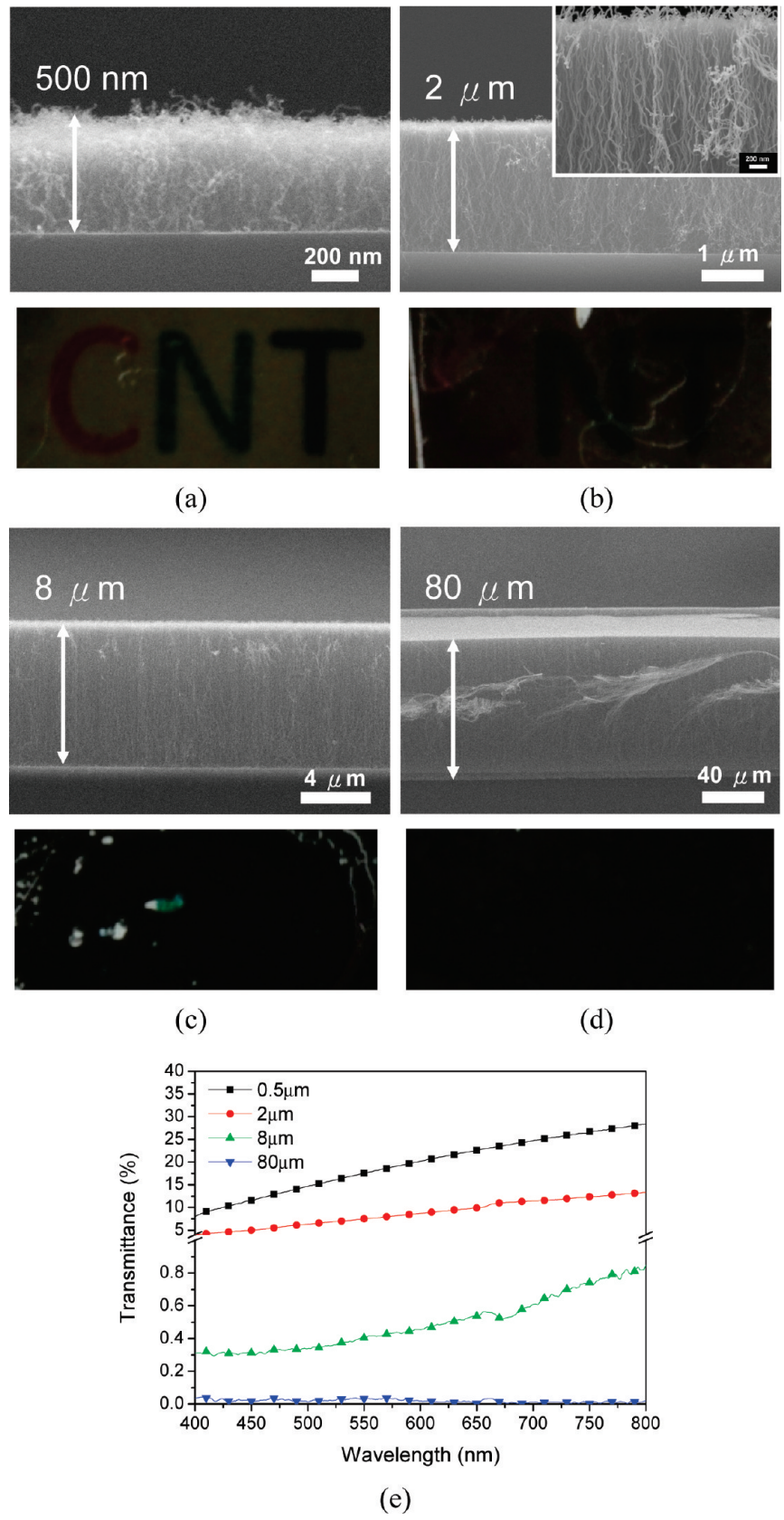


**Figure 2. SEM images and photographs of the letters "CNT" under the VA-CNT films having lengths of (a) 0.5, (b) 2 (inset: magnification of the VA-CNT tips), (c) 8, and (d) 80 μm. (e) Transmittance spectra of VA-CNT films of various lengths on PC substrates.**

$$0 = (100 - f)[(n_g^2 - n_e^2)/(n_g^2 + 2n_e^2)] + f[(n_a^2 - n_e^2)/(n_a^2 + 2n_e^2)] \quad (1)$$

where $n_g$, $n_a$, and $n_e$ are the complex refractive indices of the graphite-like material (host), air (inclusion), and the effective medium, respectively, and $f$ represents the volume fraction of the included air. In this calculation, the filling fraction of the CNTs in the 2 μm VA-CNT film was *ca.* 10%. We estimated the density of the VA-CNT films from SEM images; the air fraction (*ca.* 82%) corresponded with the calculated value obtained using the effective medium approximation and optical measurements.

Figure 3a displays the measured reflectance spectra of VA-CNT films of various thicknesses on Si substrates. In the reflectance spectrum of the 2 μm VA-CNT film with sinusoidal variation, we estimated the optical constants using the "envelope method" for an absorbed film. Thus, we calculated the refractive index and extinction coefficient from the sinusoidal interference spectrum of the 2 μm VA-CNT film. As indicated by the solid line in Figure 3a, the simulated reflectance spectrum was obtained from the calculated optical constants. The slight difference between the measured and simulated spectra in the short wavelength regime was caused by the roughness of the VA-CNT surface; that is, the surface roughness induced an interference phenomenon to disappear in the short wavelength regime. Besides, the measured ultralow-reflection spectra of the VA-CNT films having a length of 8 and 80 μm were also agreeable with the simulated results though there was a small difference due to the limit of measurement. Figure 3b reveals the refractive index and extinction coefficient of the 2 μm VA-CNT films in the visible wavelength regime; these values could be used for further optical simulation. The calculated optical constants $n$ and $k$ of the VA-CNT film at 633 nm were *ca.* 1.07 and 0.038, respectively. The refractive index of 1.07 indicates that most of the VA-CNT film was air ($n = 1$); the extinction coefficient of 0.038 is much smaller than the extinction coefficients of most metal films, even a Si film, in the visible regime. Thus, the VA-CNT film has finite absorption property, but it is not the most absorbent material. Previous reports[3] have declared that VA-CNT films are the darkest known materials, implying that the incident light is totally absorbed without any transmission or reflection. In this present study, we found that some limitations are imposed upon this darkest material. First, the thickness of the VA-CNT films must be sufficiently thick such that the transmission of light can be ignored. Second, if the VA-CNT film is coated on a substrate, then the CNT film should also be sufficiently thick that it can absorb all of the light reflected from the substrate. As indicated in Figure 3, we measured a reflectance of *ca.* 3% from the VA-CNT film having a thickness of 2 μm. This reflected light arose from the incident light penetrating the VA-CNT film, reflecting off the Si substrate, and then passing through the VA-CNT film again. Therefore, we observed both reflected and transmitted light in the VA-CNT film having a thickness of 2 μm.

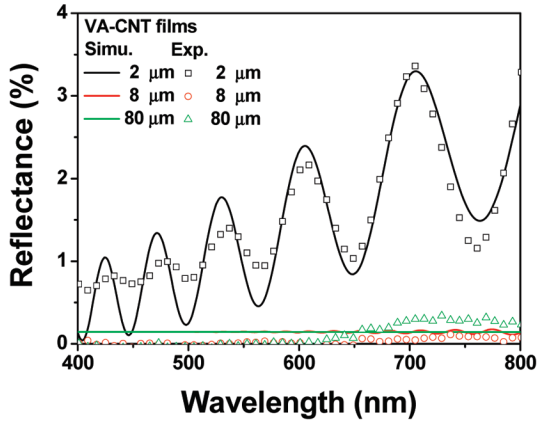


(a)

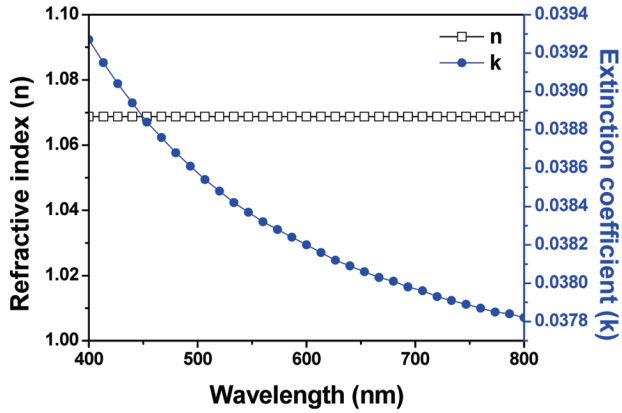


(b)

**Figure 3. (a) Reflectance spectra of VA-CNT films of various lengths on Si substrates. (b) Optical constants of the VA-CNT film having a length of 2 μm.**

Figure 2 reveals that the transmission of light vanished and the letters "CNT" underneath changed from semitransparent to dark upon increasing the thickness of the VA-CNT film. We attribute this phenomenon to the incident light being trapped and gradually absorbed by the CNT forest comprising longer CNTs. Besides, Figure 2e displays a transmission spectrum corresponding to the optical images of Figure 2a−d. Especially, the letters "CNT" in Figure 2c,d were completely vanished because the transmittance values of the CNT films were dropped to less than 1%. As evidence, a part of the green letter "N" can be seen through the scraped defect of the CNT film as shown in Figure 2c; however, nothing can be seen through the complete CNT film having a thickness of 8 μm. As displayed in Figure 3a, the interference phenomenon in the sinusoidal reflectance spectra is absent in the thick VA-CNTs films. When the VA-CNTs films in Figures 2 and 3 were sufficiently thick to prevent light from passing

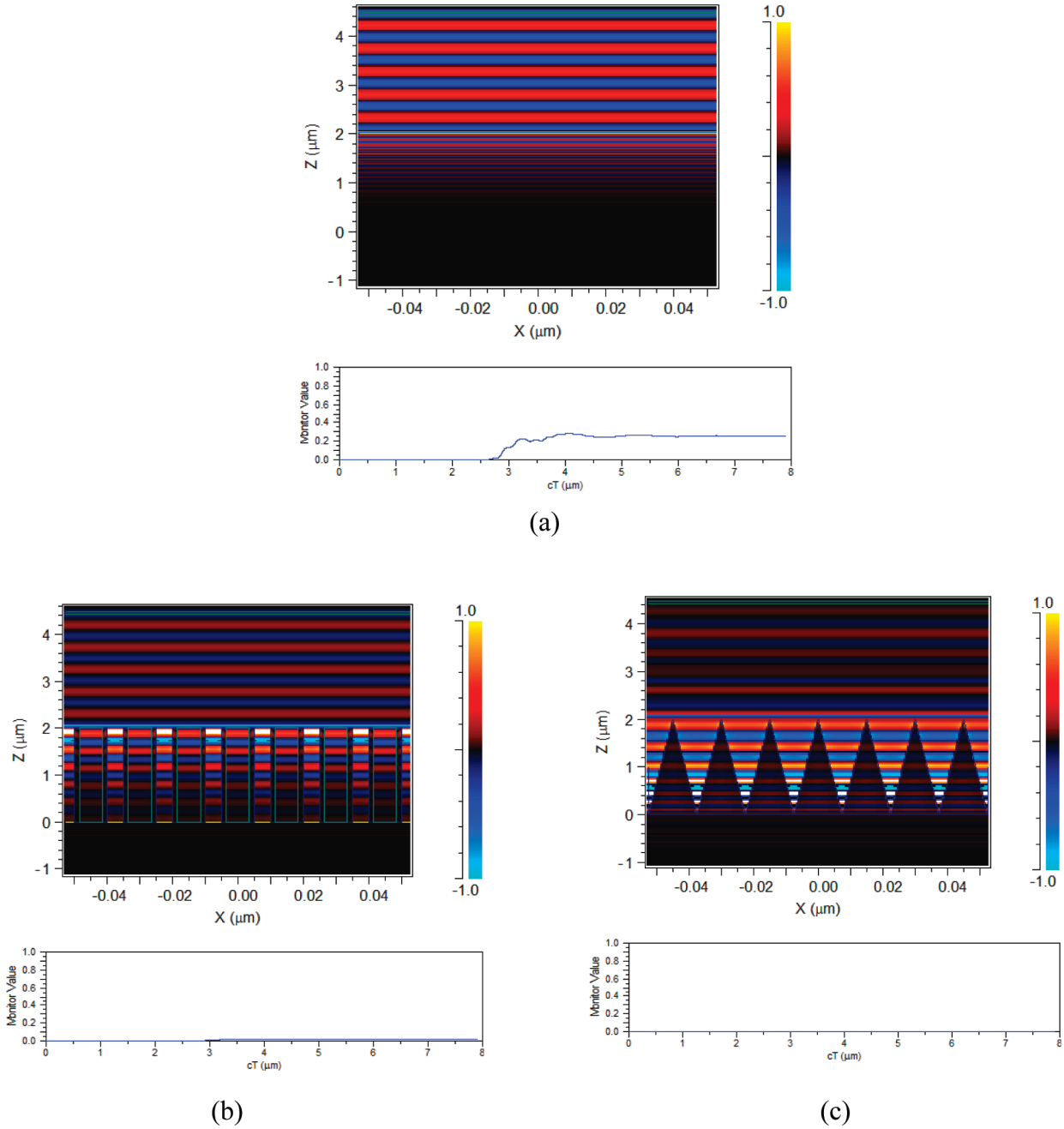


**Figure 4. Plane waves propagated from 1 μm above the air−structure interface to Si substrates (a) without structure and (b, c) possessing (b) VA-CNTs and (c) pyramidal structures having a period of 15 nm and a height of 2 μm.**

through the CNT forest, they appeared dark and had extremely low reflection.

To study the optical behavior of light within the near-field regime propagating on the VA-CNTs structure, we used the three-dimensional finite difference time domain (FDTD) method to analyze nonclose packed VA-CNTs. The FDTD is a rigorous solution to Maxwell's equations and does not have any approximations or theoretical restrictions.[30−32] Moreover, the FDTD simulations were widely used to analyze the near-field optical behavior when an incident light propagated to an antireflection structure.[33−35] In this study, the surface reflection from the VA-CNT films was simulated by the three-dimensional FDTD method that was used in the previous study of antireflection structures for solar cells. As indicated in Figure 4, a plane wave having a wavelength of 475 nm was propagated from 1 μm above the air-structure interface to the Si surface in either the presence or absence of VA-CNTs structures. The entire electric field above a value of *z* equal to 1 μm was contributed by the light reflected from the air−structure−substrate interfaces. Figure 4a displays the plane wave that propagated to the air−silicon surface in the absence of VA-CNTs structures. The apparent reflection electric field existed above the Si surface. Figure 4b displays a plane wave that propagated to the

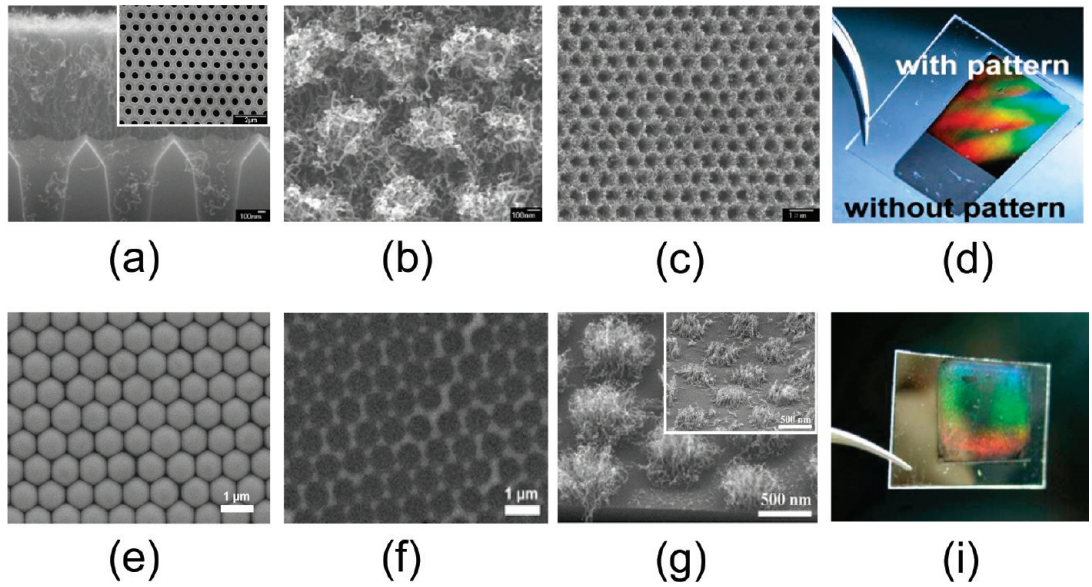


**Figure 5. (a) CNTs grown on hexagonal-Si template (inset, SEM image of hexagonal-Si template having a hole diameter of 400 nm and a period of 800 nm); (b) CNTs on the template transferred to a PC substrate; (c) surface morphology of the hexagonally patterned CNT film on a PC substrate after performing the adhesion and lift-off process; (d) color photograph of the reflection of light from the CNT film featuring the hexagonal holes pattern on a PC substrate; (e) monolayer of PS spheres having a diameter of 1 μm, arranged in hexagonal close-packed arrays; (f) honeycomb pattern of a Mo film formed on the Si substrate; (g) SEM image of broccoli-shaped CNTs on a Si substrate; (inset, broccoli-shaped CNTs transferred to a PC substrate); (h) color photograph of the reflection of light from the broccoli-shaped CNT film on a PC substrate.**

VA-CNTs having a diameter of 10 nm, a period of 15 nm, and a height of 2 μm; the reflection field was reduced significantly. The simulations suggest that the reflectance dropped from 25.5% to 1.9% after adding the VA-CNTs on a Si substrate; this change is comparable with the measured value from Figure 3. Recently, subwavelength moth-eye structures serving as antireflection coatings have attracted much attention.[36−38] Such natural antireflection structures are a superior solution toward suppressing Fresnel reflection. By combining a refractive index gradient with light trapping, Si moth-eyes structures can maintain their antireflective ability over a broad range of wavelengths of incoming light.[38] Here, we also used the three-dimensional FDTD method to simulate pyramidal Si structures having the same period (15 nm) and height (2 μm) as the VA-CNTs. Figure 4c reveals that only a small reflection field existed above the pyramidal Si structures. The simulation suggested that the reflectance dropped to 0.2% after adding the pyramidal Si structures; this value is smaller than that of the VA-CNTs of the same period and height in Figure 4b. This result demonstrates that there is another limitation for the darkest material formed from VA-CNTs: the length of the VA-CNTs should be sufficiently long to absorb all of the incoming light.

Figure 5 displays SEM and photographic images of the patterned CNT forests on flexible substrates. The inset to Figure 5a reveals a Si template with a hexagonal pattern having a period, hole-diameter, and depth of *ca.* 800, 400, and 500 nm, respectively. As indicated in Figure 5a, we grew the VA-CNT films on the patterned template by using the rapid heating CVD process. The CNTs were no longer aligned well, with some of them intertwining on the hexagonally patterned template. Because the template had a pyramid structure, the growth of the CNTs was affected by the tilt of the substrate planes. Although the CNTs were poorly aligned, the surface profiles of the patterns could be observed clearly. Figure 5b displays SEM images of the hexagonally patterned CNT film transferred to a flexible PC substrate. To improve the surface morphology contrast, Figure 5c presents the patterned CNT film on a PC substrate obtained after it had been adhered to and lifted off using a cellophane tape to remove the nontransferred CNTs. After performing this process, the surface morphology of the hexagonally patterned CNT film, which had a period and hole diameter of 800 and 400 nm, respectively, became clearer. Figure 5d reveals the colorful reflection from this hexagonally patterned CNT sample.

Figure 1c outlines the approach we took toward fabricating unique broccoli-shaped profiles of CNTs through NSL with a poisoned catalyst. Figure 5 panels e−h display SEM images of the samples obtained during this fabrication procedure. In Figure 5e, a monolayer of PS spheres having a diameter of 1 μm is arranged in a hexagonal close-packed (HCP) array. We deposited a Mo layer on top of the PS spheres and then removed the PS spheres to form a honeycomb-patterned Mo film on the Si substrate (Figure 5f). A multitarget sputter system was then used to sputter the layered Co/Ti catalyst (0.5 nm/0.5 nm) on the patterned Mo film. The presence of Mo poisoned the Co/Ti catalyst, thereby

preventing the CNTs from growing on the sites occupied by the Mo metal. As a result, we obtained a hexagonal array of broccoli-shaped CNTs. Figure 5g reveals that each broccoli-shaped CNT had a diameter of *ca.* 700 nm and a height of *ca.* 500 nm. The inset to Figure 5g displays the broccoli-shaped CNTs after they had been transferred to the flexible PC substrate. The catalyst and Mo layer remained on the Si substrate and did not influence the iridescence of the CNTs on the PC substrate. The images of the honeycomb-structured CNTs in Figure 5c and the broccoli-shaped CNTs in Figure 5g are readily distinguishable. The method we used to fabricate the broccoli-shaped CNTs is known as inverse nanosphere lithography (INSL). Large-area patterned CNT arrays were obtained using the INSL process, with the boundaries of the broccoli-shaped CNTs corresponding to the domain boundaries of the PS spheres. Figure 5h reveals the colorful image of the film of the broccoli-shaped CNTs.

The AFM image in Figure 6a displays the surface morphology—namely the honeycomb pattern of the Mo layer—of the sample used to obtain the SEM image in Figure 5f. Defect positions in the original PS sphere monolayer appeared as deposited Mo ridges. The diameter of each hole was *ca.* 800 nm, slightly smaller than the average diameter of the PS spheres, presumably due to the deposition of high-mobility Mo ions beneath the spheres. To investigate the effect of the catalyst-poisoning Mo layer on CNT growth, we prepared three samples having different coatings on Si substrates: one was a coating of Co/Ti/Mo (0.5 nm/0.5 nm/100 nm) and the other two were coatings of Co/Ti (0.5 nm/0.5 nm). The Co/Ti/Mo sample and one of the Co/Ti samples were annealed at 700 °C, while the other Co/Ti sample was maintained at room temperature. Figure 6b presents the XPS spectra of these samples. The peaks are assigned for each element according to their binding energies. Prior to annealing, only signals for Co atoms were evident for the sample lacking the Mo coating; both Co and Ti peaks were present after annealing. In contrast, the peaks for the Co atoms disappeared after annealing the sample coated with the Mo layer. The inactivation of the Co catalyst presumably arose from the diffusion of Co atoms into the Mo layer during the high temperature of the CNT growth process. This result suggests that the Co/Mo ratio is a critical feature controlling the extent of CNT synthesis. A suitable

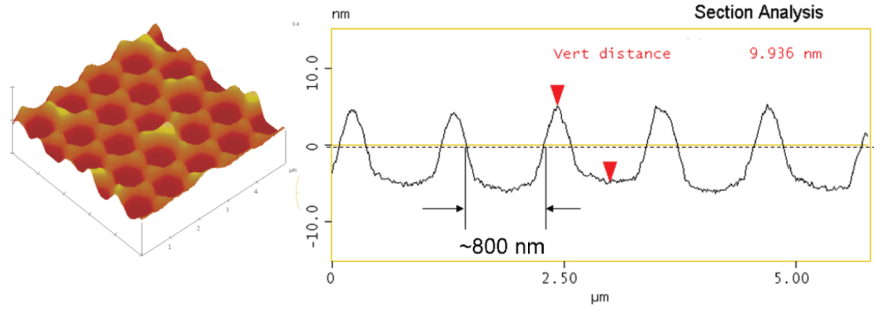


(a)

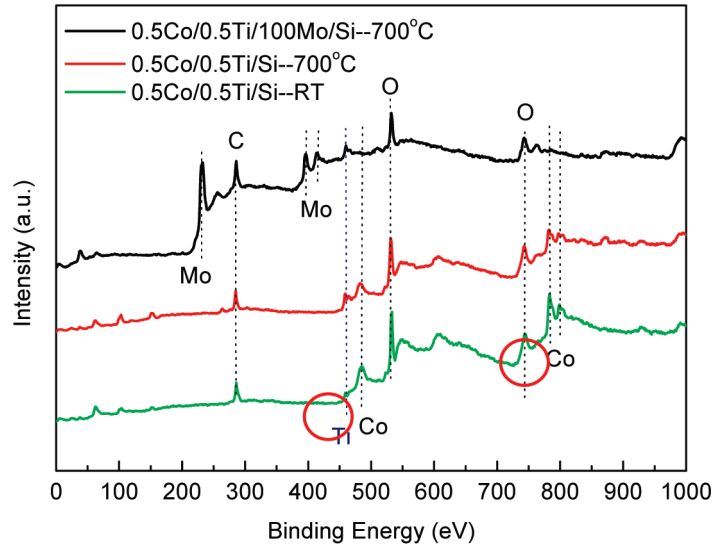


(b)

**Figure 6. (a) Surface morphology of the honeycomb-patterned Mo film; (b) XPS spectra of the Co/Ti catalyst coated on Si substrates, with and without the Mo layer, before and after annealing.**

ratio promotes CNT synthesis, whereas a high Mo content results in a poisoned catalyst and suppressed CNT growth. In this study, we fabricated a unique broccoli-shaped profile of CNTs through NSL using a poisoned-catalyst mechanism.

To study the optical behavior of the colorful CNTs, we measured the diffraction spectra from normal incident light and after changing the detection angle. As displayed in Figure 7a, the diffraction spectra of the CNTs featuring the hexagonal hole pattern red-shifted upon increasing the detection angle. Thus, the colorful image of the patterned CNTs arose from the diffraction of light from the periodical CNT forests. Figure 7a also displays the diffraction spectra of the patterned CNT film on the PC plate, before and after performing the adhesion and lift-off process. After removing the non-transferred CNTs using Scotch tape, the diffraction intensity increased dramatically as a result of a reduction in the amount of randomly scattered light. We can use the diffraction theory to explain the peak shift, which is described in the following equation[39]

$$m\lambda = (\sqrt{3}/2)P(\sin\theta_1 + \sin\theta_2) \qquad (2)$$

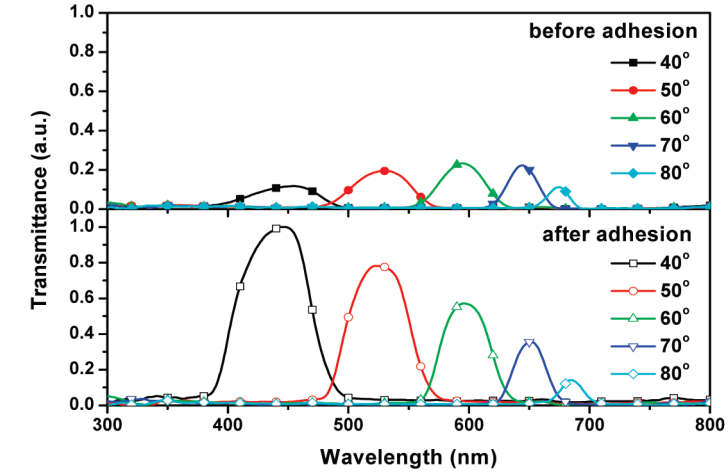


(a)

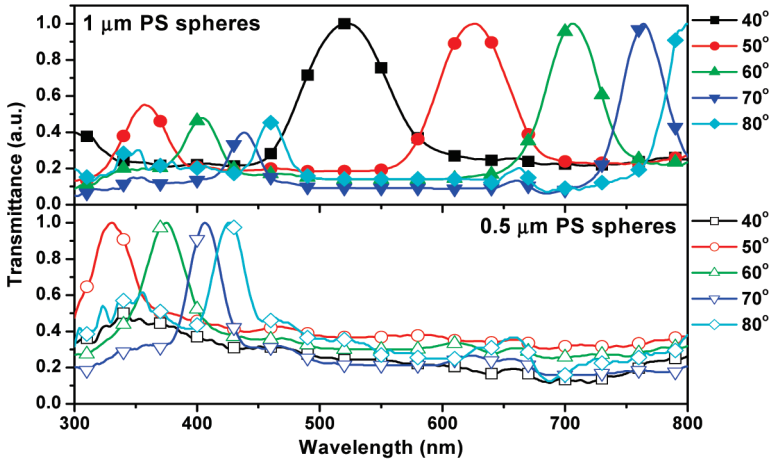


(b)

**Figure 7. (a) Diffraction spectra of films of CNTs featuring hexagonal-hole patterns on a PC plate before (top) and after (bottom) performing the adhesion and lift-off process. (b) Diffraction spectra of broccoli-shaped CNTs prepared using templates of PS spheres having diameters of 1 μm (top) and 0.5 μm (bottom).**

where λ is the diffraction peak wavelength, $\theta_1$ and $\theta_2$ are the incident and diffraction angles, *P* is the period, and *m* is an integer. In the CNTs possessing hexagonal-hole patterns, the theoretical peak wavelengths at diffraction angles of 40, 50, 60, 70, and 80° are 445, 530, 600, 651, and 682 nm, respectively. Thus, the measured values of the peak wavelengths agree well with the theoretical values.

The top and bottom traces in Figure 7b are the diffraction spectra of the broccoli-shaped CNTs prepared using templates of PS spheres having average diameters of 1 and 0.5 μm, respectively. The diffraction peak wavelengths of the broccoli-shaped CNTs having a period of 1 μm are approximately twice those of the broccoli-shaped CNTs having a period of 0.5 μm. The diffraction peaks shifted to longer wavelengths upon increasing the detection angle. The measured peak wavelengths also agree well with the theoretical values for both sets of broccoli-shaped CNTs. These results indicate that the colorful images arose from the diffraction of light from the periodical arrays of CNTs, even though CNTs are high absorption materials, and from the low contrast between the refractive indices of the CNT film ($n = ca.$ 1.07) and air ($n = ca.$ 1). Because the VA-CNTs trapped the incident light in the CNT forests almost without any reflection, transmission, or scattering, the previous study[3] called them the "darkest material." We have found, however, that the darkest VA-CNT surfaces must be sufficiently thick to prevent light from transmitting or reflecting from the surface of the substrates. We observed that patterned CNTs were colorful, possibly due to the leakage of light of a different optical phase as it passed through the patterned CNT forest. Although the contrast between the refractive indices of the CNT film and air was low, constructive or destructive interference could still occur in CNTs featuring periodical patterns, thereby inducing iridescence phenomena.

## CONCLUSIONS

We examined CNT forests exhibiting two types of optical properties: those of "darkest materials" and those of iridescence phenomena. The VA-CNT forests behaving as darkest materials exhibited extremely low reflection, which was caused by light trapping and absorption in the CNT forests. Nevertheless, the thicknesses of CNT forest must be chosen carefully to prevent light from transmitting through the CNT forest or reflecting from the substrate. The calculated optical constants *n* and *k* of the VA-CNTs film at the wavelength of 633 nm were *ca.* 1.07 and 0.038, respectively. The low refractive index indicates that most of the VA-CNT film was air; the extinction coefficient of the VA-CNT film was much smaller than the extinction coefficients of most metal films, even a Si film, in the visible regime. Thus, the VA-CNT films had finite absorption, but they were not the most absorbent materials. The limitation of a darkest material featuring CNT forests requires that the length of the VA-CNTs should be greater than *ca.* 10 μm if they are to entirely absorb the transmitted light. On the basis of the FDTD simulation, we also found that the reflectance from Si moth's eye structures was smaller than that from VA-CNTs having the same period and height. To study the iridescence of the CNTs, we prepared two kinds of patterned CNT forests on flexible PC substrates: a CNT array featuring hexagonal-hole patterns and a broccoli-like CNT array, the latter being prepared using INSL in conjunction with a poisoned-catalyst mechanism. In the patterned CNT forests, even though the difference between the refractive indices of the CNT film and air was extremely low and even though the CNTs could trap incident

light, the iridescence phenomenon remained to induce colorful CNT images. The iridescence of patterned CNT forests can be applied in various flexible devices, such as solar cells and displays.

## METHODS

**VA-CNTs Synthesis.** The catalysts were prepared in layered forms and deposited using a general sputtering method. A layered Co/Ti catalyst (0.5 nm/0.5 nm) was sputtered on the patterned substrates using a multitarget DC-power sputtering system. The sample was then placed in a cold-wall of a rapid heating and cooling chemical vapor deposition (CVD) chamber, which was evacuated to 3 mtorr prior to CNT growth. A mixture of $H_2$ and Ar (1:9), the reduction agent and buffer gas, respectively, was introduced into the reactor at the pressure of 10 Torr. The sample was heated from room temperature to the processing temperatures (500−800 °C) within 2 min, and then it was maintained at that temperature for 5 min. Then $C_2H_2$ gas was channeled into the reactor at a flow rate of 60 sccm to grow the CNTs for 5 min.[28] The density was manually calculated from the enlarged SEM images. The characterization of the CNTs was reported in our previous work.[40] The CNTs were analyzed by a high resolution transmission electronic microscope (HRTEM). We found that the CNTs have a multiwalled structure and a diameter of *ca.* 10 nm.[40]

**Synthesis of CNTs Aligned with Hexagonal Holes.** The patterned Si templates were fabricated using sequential electron beam lithography and reactive ion etching. A high density plasma reactive ion etching (HDP-RIE) system (Duratek, Multiplex Cluster) equipped with an inductively coupled plasma (ICP) source was used to fabricate the hexagonally patterned template. The template was composed of periodic holes, 400 nm in diameter and 800 nm in period.

**Broccoli-Shaped CNTs Synthesis.** The Si substrate was cleaned with deionized water in an ultrasonic bath for 10 min, and then it was treated hydrophilically at 70 °C for 45 min. The solution for hydrophilic treatment was made from 500 mL of deionized water, 100 mL of hydrogen peroxide ($H_2O_2$, 26%), and 100 mL of ammonia ($NH_4OH$, 38%). A 10 wt % solution of monodisperse PS spheres (Microparticles GmbH, Germany) was mixed with methanol at a volume ratio of 4:1. A drop of the mixed solution was placed on the hydrophilic Si substrate, following spinning of the substrate at a controlled rate of 800 rpm for 60 s. Once a monolayer of the close-packed PS sphere array was obtained, a thin film of Mo having a thickness of 100 nm was sputtered onto the periodically patterned PS spheres. The PS spheres were removed from the Si substrate through ultrasonic cleaning, and then the substrate was dried under $N_2$ gas.

**Transferring to PC Substrates.** To transfer the CNT forests onto a flexible substrate, a PC plate was placed on the top of the VA-CNTs, and then the sample was heated at 150 °C for 5 min under a pressure of 1 MPa.

**Characterization.** The Si and flexible substrates presenting the patterned CNT forests were examined using a field-emission scanning electron microscope (FE-SEM, JEOL-6500F); the surface profile was observed using an atomic force microscope (AFM, Digital Instrument-DI3100). Surface analysis was performed using X-ray photoelectron spectroscopy (XPS, HPI 1600) to investigate the influence of the Mo layer on the activity of the Co/Ti catalyst. The optical spectra were measured using a Hitachi U4100 spectrophotometer.

*Acknowledgment.* We thank the National Science Council, Taiwan, R.O.C., for supporting this study under contracts NSC-97-2221-E-002-046-MY3 and NSC-97-2623-7-002-008-ET.

## REFERENCES AND NOTES

1. Garcia-Vidal, F. J.; Pitarke, J. M.; Pendry, J. B. Effective Medium Theory of the Optical Properties of Aligned Carbon Nanotubes. *Phys. Rev. Lett.* **1997**, *78*, 4289–4292.
2. de los Arcos, T.; Oelhafen, P.; Mathys, D. Optical Characterization of Alignment and Effective Refractive Index in Carbon Nanotube Films. *Nanotechnology* **2007**, *18*, 265706.
3. Yang, Z. P.; Ci, L.; Bur, J. A.; Lin, S. Y.; Ajayan, P. M. Experimental Observation of an Extremely Dark Material Made By a Low-Density Nanotube Array. *Nano Lett.* **2008**, *8*, 446–451.
4. Kodama, S.; Horiuchi, M.; Kunii, T; Kuroda, K. Ultra-black Nickel-Phosphorus Alloy Optical Absorber. *IEEE Trans. Instrum. Meas.* **1990**, *39*, 230–232.
5. Shirley, L. G.; George, N. Diffuser Radiation Patterns over a Large Dynamic Range. 1: Strong Diffusers. *Appl. Opt.* **1988**, *27*, 1850–1860.
6. Brown, R. J. C.; Brewer, P. J.; Milton, M. J. T. The Physical and Chemical Properties of Electroless Nickel-Phosphorus Alloys and Low Reflectance Nickel-Phosphorus Black Surfaces. *J. Mater. Chem.* **2002**, *12*, 2749–2754.
7. Burmeister, F.; Schäfle, C.; Keilhofer, B.; Bechinger, C.; Boneberg, J.; Leiderer, P. From Mesoscopic to Nanoscopic Surface Structures: Lithography with Colloid Monolayers. *Adv. Mater.* **1998**, *10*, 495–497.
8. Chen, X.; Chen, Z.; Fu, N.; Lu, G.; Yang, B. Versatile Nanopatterned Surfaces Generated *via* Three-Dimensional Colloidal Crystals. *Adv. Mater.* **2003**, *15*, 1413–1417.
9. Tan, T. L.; Wong, D.; Lee, R. Iridescence of a Shell of Mollusk *Haliotis glabra*. *Opt. Express* **2004**, *12*, 4847–4854.
10. Jewell, S. A.; Vukusic, P.; Poberts, N. W. Circularly Polarized Colour Reflection from Helicoidal Structures in the Beetle Plusiotis Boucardi. *J. Phys. (Paris)* **2007**, *9*, 99.
11. Huang, J. Y.; Wang, X. D.; Wang, Z. L. Controlled Replication of Butterfly Wings for Achieving Tunable Photonic Properties. *Nano Lett.* **2006**, *6*, 2325–2321.
12. Li, Y.; Li, C. C.; Cho, S. O.; Duan, G. T.; Cai, W. P. Silver Hierarchical Bowl-Like Array: Synthesis, Superhydrophobicity, and Optical Properties. *Langmuir* **2007**, *23*, 9802–9807.
13. Nilsson, L.; Groening, O.; Emmenegger, C.; Kuettel, O.; Schaller, E.; Schlapbach, L.; Kind, H.; Bonard, J. M.; Kern, K. Scanning Field Emission from Patterned Carbon Nanotube Films. *Appl. Phys. Lett.* **2000**, *76*, 2071–2073.
14. Milne, W. I.; Teo, K. B. K.; Chhowalla, M.; Amaratunga, G. A. J.; Pribat, D.; Legagneux, P. Electron Emission from Arrays of Carbon Nanotubes/Fibres. *Curr. Appl. Phys.* **2002**, *2*, 509–513.
15. Semet, V.; Binh, V. T.; Vincent, P.; Guillot, D.; Teo, K. B. K.; Chhowalla, M. Field Electron Emission from Individual Carbon Nanotubes of a Vertically Aligned Array. *Appl. Phys. Lett.* **2002**, *81*, 343–345.
16. Wang, W.; Summers, C. J.; Wang, Z. L. Large-Scale Hexagonal-Patterned Growth of Aligned ZnO Nanorods for Nano-optoelectronics and Nanosensor Arrays. *Nano Lett.* **2004**, *4*, 423–426.
17. Vlasov, Y. A.; Bo, X. Z.; Sturm, J. C.; Norris, D. J. On-Chip Natural Assembly of Silicon Photonic Bandgap Crystals. *Nature* **2001**, *414*, 289–293.
18. Arsenault, A. C.; Clark, T. J.; Von Freymann, G.; Cademartiri, L.; Sapienza, R.; Bertolotti, J.; Vekris, E.; Wong, S.; Kitaev, V.; Manners, I.; *et al*. From Colour Fingerprinting to the Control of Photoluminescence in Elastic Photonic Crystals. *Nat. Mater.* **2006**, *5*, 179–184.
19. Kempa, K.; Kimball, B.; Rybczynski, J.; Huang, Z. P.; Wu, P. F.; Steeves, D.; Sennett, M.; Giersig, M.; Rao, D. V. L. N.; Carnahan, D. L.; *et al*. Photonic Crystals Based on Periodic Arrays of Aligned Carbon Nanotubes. *Nano Lett.* **2003**, *3*, 13–18.
20. Rybczynski, J.; Kempa, K.; Wang, Y.; Zen, Z. F.; Carlson, J. B.; Kimball, B. R.; Benham, G. Visible Light Diffraction Studies on Periodically Aligned Arrays of Carbon Nanotubes: Experimental and Theoretical Comparison. *Appl. Phys. Lett.* **2006**, *88*, 203122.
21. Correa-Duarte, M. A.; Kosiorek, A.; Kandulski, W.; Giersig, M.; Liz-Marzan, L. M. Layer-by-Layer Assembly of Multiwall Carbon Nanotubes on Spherical Colloids. *Chem. Mater.* **2005**, *17*, 3268–3272.

22. Wang, X.; Neff, C.; Graugnard, E.; Ding, Y.; King, J. S.; Pranger, L. A.; Tannenbaum, R.; Wang, Z. L.; Summers, C. J. Photonic Crystals Fabricated Using Patterned Nanorod Arrays. *Adv. Mater.* **2005**, *17*, 2103–2106.
23. Kei, C.-C.; Chen, T.-H.; Chang, C.-M.; Su, C. Y.; Lee, C.-T.; Hsiao, C.-N.; Chang, S.-C.; Perng, T.-P. Preparation of Periodic Arrays of Metallic Nanocrystals by Using Nanohoneycomb as Reaction Vessel. *Chem. Mater.* **2007**, *19*, 5833–5835.
24. Kosiorek, A.; Kandulski, W.; Glaczynsha, H.; Giersig, M. Fabrication of Nanoscale Rings, Dots, and Rods by Combining Shadow Nanosphere Lithography and Annealed Polystyrene Nanosphere Masks. *Small* **2005**, *1*, 439–444.
25. Weekes, S. M.; Orgin, F. Y.; Murray, W. A. Fabrication of Large-Area Ferromagnetic Arrays Using Etched Nanosphere Lithography. *Langmuir* **2004**, *20*, 11208–11212.
26. Wang, B.; Zhao, W.; Chen, A.; Chua, S. J. Formation of Nanoimprinting Mould through Use of Nanosphere Lithography. *J. Cryst. Growth* **2006**, *288*, 200–204.
27. Wang, Y.; Wang, X.; Rybczynski, J.; Wang, D. Z.; Kempa, K.; Ren, Z. F. Triangular Lattice of Carbon Nanotube Arrays for Negative Index of Refraction and Subwavelength Lensing Effect. *Appl. Phys. Lett.* **2005**, *86*, 153120.
28. Chiu, C. C.; Tsai, T. Y.; Tai, N. H. Field Emission Properties of Carbon Nanotube Arrays through the Pattern Transfer Process. *Nanotechnology* **2006**, *17*, 2840–2844.
29. Bruggemann, D. A. G. Calculation of Various Physics Constants in Heterogenous Substances. I. Dielectricity Constants and Conductivity of Mixed Bodies from Isotropic Substances. *Ann. Phys.* **1935**, *24*, 636–664.
30. Berenger, J. P. A Perfectly Matched Layer for the Absorption of Electromagnetic Waves. *J. Comput. Phys.* **1996**, *114*, 185–200.
31. Taflove, A.; Hagness, S. C. *Computational Electrodynamics: The Finite-Difference Time-Domain Method*; Artech House: Norwood, MA, 1995.
32. Yee, K. S. Numerical Solution of Initial Boundary Value Problems Involving Maxwell's Equations in Isotropic Media. *IEEE Trans. Antennas Propagat.* **1966**, *14*, 302–307.
33. Chen, H. L.; Chuang, S. Y.; Lin, C. H.; Lin, Y. H. Using Colloidal Lithography to Fabricate and Optimize Subwavelength Pyramidal and Honeycomb Structures in Solar Cells. *Opt. Express* **2007**, *15*, 14793–14803.
34. Pala, A.; White, J.; Barnard, E.; Liu, J.; Brongersma, M. L. Design of Plasmonic Thin-Film Solar Cells with Broadband Absorption Enhancements. *Adv. Mater.* **2009**, *21*, 1–6.
35. Li, Z. F.; Ozbay, E.; Chen, H. B.; Chen, J. J.; Yang, F. H.; Zheng, H. Z. Resonant Cavity-Based Compact Efficient Antireflection Structures for Photonic Crystals. *J. Phys. D: Appl. Phys.* **2007**, *40*, 5873–5877.
36. Thornton, B. S. Limit of the Moth's Eye Principle and Other Impedance-Matching Corrugations for Solar-Absorber Design. *J. Opt. Soc. Am.* **1975**, *65*, 267–270.
37. Clapham, P. B.; Hutley, M. C. Reduction of Lens Reflection by Moth Eye Principle. *Nature* **1973**, *244*, 281–282.
38. Diedenhofen, S. L.; Vecchi, G.; Algra, R. E.; Hartsuiker, A.; Muskens, O. L.; Immink, G.; Bakkers, E. P. A. M.; Vos, W. L.; Rivas, J. G. Broad-band and Omnidirectional Antireflection Coatings Based on Semiconductor Nanorods. *Adv. Mater.* **2009**, *21*, 973–978.
39. Krieger, I. M.; O'Neill, F. M. Diffraction of Light by Arrays of Colloidal Spheres. *J. Am. Chem. Soc.* **1968**, *90*, 3114–3120.
40. Tsai, T. Y.; Tai, N. H.; Chen, K. C.; Lee, S. H.; Chan, L. H.; Chang, Y. Y. Growth of Vertically Aligned Carbon Nanotubes on Glass Substrate at 450 °C through the Thermal Chemical Vapor Deposition Method. *Diamond Relat. Mater.* **2009**, *18*, 307–311.